ARTICLE

Stable Electron Field Emission from PMMA−CNT Matrices

Archana Pandey, Abhishek Prasad, Jason P. Moscatello, and Yoke Khin Yap*

Department of Physics, Michigan Technological University, Houghton, Michigan 49931, United States

ABSTRACT We have created PMMA−CNT matrices by embedding opened-tip vertically aligned multiwalled carbon nanotubes (VA-MWCNTs) with poly(methyl methacrylate) (PMMA). These PMMA−CNT matrices are excellent electron field emitters with an emission threshold field of 1.675 V/μm, more than 2-fold lower that that of the as-grown sample. In addition, the emission site density from these matrices is high, merely filling up the entire sample surface. Emission stability test at ~1.35 mA/cm^2 was performed continuously for 40 h with no significant degradation. On the basis of our theoretical simulation and hypothetical modeling, we attribute these performances to the reduced screening effect and fewer Joule heatings due to the shorter effective transport distance of the electrons in MWCNTs.

KEYWORDS: carbon nanotubes · field emission · stability · Joule heating · screening effect

For more than a decade, electron field emission has been recognized as a promising application of carbon nanotubes (CNTs).[1−5] This is due to the high aspect ratios, good thermal and electrical conductivity, and robust chemical and mechanical stability of CNTs. However, reliable commercial electron field emitters based on CNTs are still not available. Apparently, device lifetime, long-term emission stability, and low emission density are the major issues for practical field emission devices. Many techniques have been studied to enhance the performance of multiwalled carbon nanotubes (MWCNTs) for electron field emission.[6−8] Some attempted to modify the properties of CNTs by coating with metal oxide (In_2O_3), wide band gap materials, polymer, MgO, and barium strontium oxide.[9−13] Most of these works focused on reducing the threshold electric field for emission. However, device lifetime, long-term emission stability, and emission density are scarcely discussed. Poor device lifetime due to resistive heating and mechanical failure at the interface of CNTs/substrate has been reported.[14] On the other hand, recent work starts to evaluate the fundamental factors behind stable field emission and high emission density. We found that the graphitic order of CNTs is one of the key factors for stable field emission.[15] Recently, we show that *both* emission stability and density can be enhanced by self-organized opened-tip CNT bundles.[16]

We report here that PMMA−CNT matrices are excellent electron field emitters with all the desired properties, such as low emission threshold field, prolonged emission stability, and high emission density. We refer to PMMA−CNT matrices as arrays of opened-tip vertically aligned multiwalled carbon nanotubes (VA-MWCNTs) embedded with poly(methyl methacrylate) (PMMA). We found that the emission thresholds (E_{th}, electric field required for an emission current density of 1 μA/cm^2) of PMMA−CNT matrices can be more than 2-fold lower than that of the as-grown VA-MWCNTs. Furthermore, PMMA−CNT matrices can continue to emit electrons for 40 h with negligible degradation. These PMMA−CNT matrices also have very uniform and dense emission sites. Descriptions on sample preparation and field emission characterization are given in the Methods (Figure 1).

RESULTS AND DISCUSSION

Figure 2 shows the scanning electron microscope (SEM) images and the related Raman spectroscopy for our samples. All of these samples have VA-MWCNTs of ~4 μm length and ~40 nm diameter (Figure 2a). Figure 2b shows that the as-grown VA-MWCNTs can be fully embedded in PMMA after the dip coating and curing processes. Magnified SEM view on the embedded sample was obtained after coating the sample with a thin layer (<1 nm) of Au

*Address correspondence to ykyap@mtu.edu.

Received for review April 28, 2010 and accepted October 04, 2010.

Published online October 18, 2010. 10.1021/nn100925g

film to reduce the charging effects on PMMA. As shown, VA-MWCNTs are embedded and not visible under SEM. Opened-tip VA-MWCNTs are exposed on the top surface of the PMMA−CNT matrix after polishing (Figure 2c). The corresponding Raman spectra for the as-grown sample, the PMMA embedded sample, and the PMMA−CNT matrix are shown in Figure 2d−f, respectively. These Raman spectra were obtained by a confocal Raman microscope using a laser excitation wavelength of 632 nm. The graphitic, *G* (~1580 cm^{-1}), and the disorder, *D* (~1330 cm^{-1}), peaks for VA-MWCNTs in the as-grown sample are shown in Figure 2d. These peaks are diminishes in the PMMA embedded sample, and only the PMMA Raman peaks are detected (Figure 2e).[17] The *G* and *D* peaks reappeared in the PMMA−CNT matrix, as evident in Figure 2f.

Figure 3a,b shows the emission current density (*J*) *versus* the applied electric field (*E*) for the as-grown sample and the PMMA−CNT matrix. The threshold electric field, E_{th}, for the as-grown sample was found to be 3.898 V/μm (Figure 3a). This threshold was reduced to 1.675 V/μm for the PMMA−CNT matrix (Figure 3b). Similar trend has been detected from six sets of samples. E_{th} for the as-grown samples can be as high as 4.4 V/μm and can be as low as 1.0 V/μm for the matrices. The corresponding Fowler−Nordheim (*F*−*N*) plots for these samples can be seen in Figure 3c,d. The linearity of these *F*−*N* plots confirms the phenomena of field emission. The effective enhancement factors estimated from these plots are 1172 and 4045 for the as-grown sample and the PMMA−CNT matrix, respectively. The emission site densities as collected from the fluorescence on the ITO electrode are shown in Figure 3e,f for the as-grown and the PMMA−CNT matrix, respectively. As shown, the emission site density is much higher for the PMMA−CNT matrix. Due to the relatively large anode−cathode distance (1 mm), the detected emission images are actually magnified ~1.5 times due to the divergence of the emitted electron beams (diverging angle ~23.5°). The emission density will appear to be more uniform at smaller gaps. In addition, the density near the edges of the growth area is relatively lower due to lower CNT density affected by the catalyst film thickness variation near the edges of the shadow mask. The circular shapes of the emission sites show that the electron field emission was occurring only from the areas where VA-MWCNTs were grown.

We attempt to understand the reduced E_{th} and enhance emission density from the PMMA−CNT matrix. Both E_{th} and emission density depend on the aspect ratio of the CNTs and their intertube spacing (screening effects). Since both the as-grown sample and the PMMA−CNT matrix have VA-MWCNTs with identical aspect ratios and intertube spacing, the lower E_{th} and the enhanced emission density detected from the PMMA−CNT matrix are related to the PMMA filling because opened-tip geometry alone did not significantly improve the emission properties.[16] A possible explanation is that the dielectric properties of PMMA have helped to reduce the screening effect between the CNTs. In order to verify this argument, we have simulated the screening effect of CNTs using the COMSOL Multiphysics software. The simulation parameters are as follows: diameter of CNTs, D_{CNTs} = 40 nm; length of CNTs, L_{CNTs} = 4 μm; edge to edge spacing between CNTs, S = 40 nm; applied electric field between top and bottom boundaries, E_{appl} = 5 V/μm. Simulation for an array of as-grown VA-MWCNTs (Figure 3g) shows that the CNT at the center has the lowest local electric field due to the screening effects from the neighboring CNTs (~9.89×10^6 V/m at point 1, ~6.21×10^6 V/m at point 2, and ~9.42×10^6 V/m at point 3). The enhancement factors are thus ~2 due to the screening effect of surrounding CNTs. The enhancement factors estimated from the actual *F*−*N* plots are higher since not all nanotubes in the samples contributed to the collected currents. Next, we simulate for the case of the PMMA−CNT matrix. The spaces between VA-MWCNTs are now simulated to have a dielectric constant, $\boldsymbol{k}$ = 3.4.[18] As shown in Figure 3h, the local field at the center of the PMMA−CNT matrix is ~45% higher as compared with those of as-grown VA-MWCNTs (point 2: ~7.76×10^6

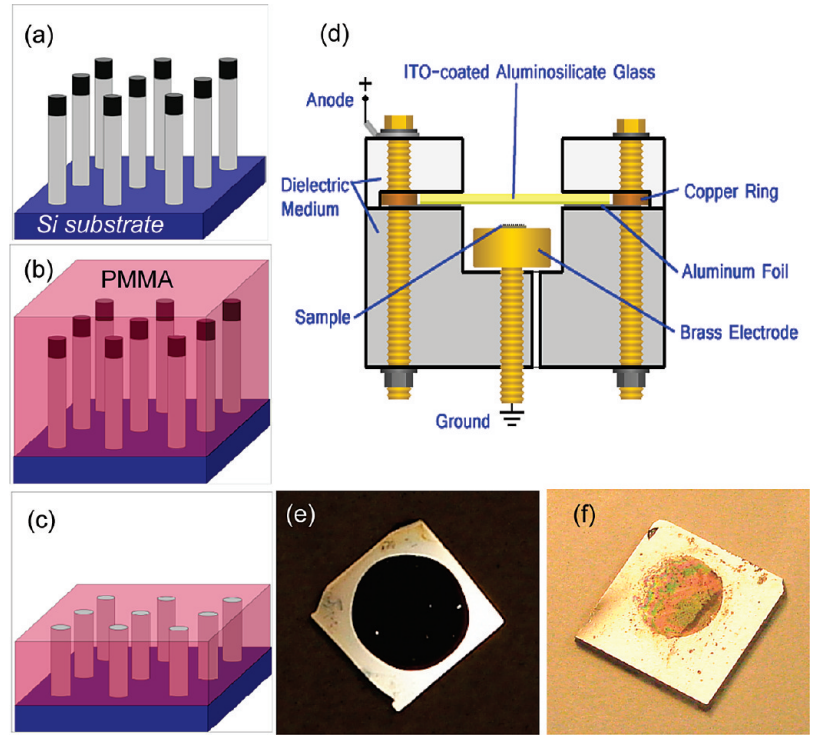

Figure 1. Schematic for the fabrication of PMMA−CNT matrices. (a) As-grown VA-MWCNTs on a Si substrate with Ni nanoparticles at their tips. (b) VA-MWCNTs embedded with PMMA. (c) PMMA−CNT matrix with opened-tip VA-MWCNTs after mechanical polishing. (d) Schematic of the field emission setup. Appearances of the (e) as-grown sample and the (f) PMMA−CNT matrix. The darker circular regions at the centers are as-grown VA-MWCNTs (e) and VA-MWCNTs embedded in PMMA after polishing (f).

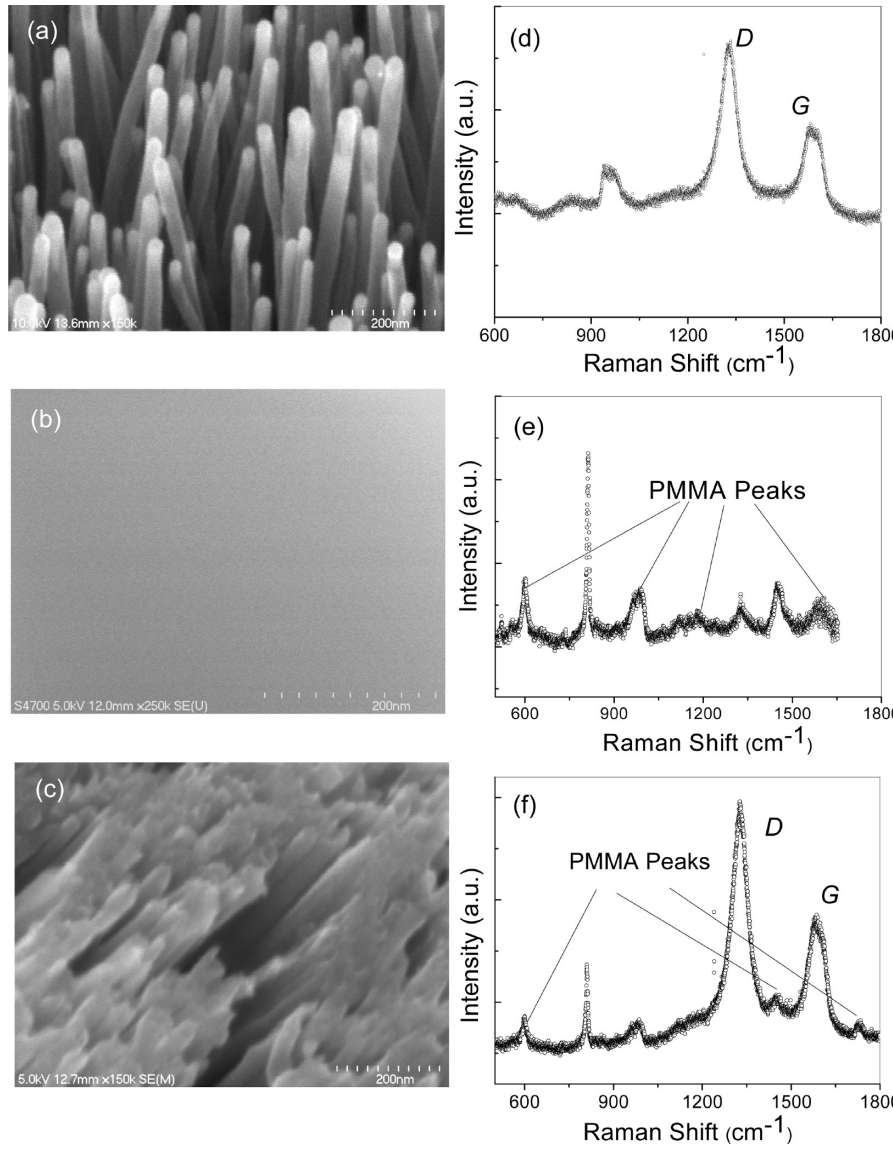

Figure 2. SEM images of (a) the as-grown sample, (b) sample embedded in PMMA, and (c) PMMA−CNT matrix with exposed CNT tips. (d−f) Corresponding Raman spectra.

V/m). The local fields at the edges of the matrix (point 1: ~1.04 × 10^7 V/m, point 3: ~1.06 × 10^7 V/m) are also slightly increased (~4.9 and ~11.3%, respectively). Apparently, PMMA filling can reduce the screening effects especially for areas where MWCNTs are closely packed. This may also contribute to the higher emission site density from the PMMA−CNT matrix. However, since these enhancements are moderate, we think that the reduced screening effect is not the only reason for enhanced emission properties described so far.

In fact, a reduced E_{th} was also detected by Watts *et al.*, but the mechanism behind was not explained.[11] On the other hand, Tanaka *et al.* studied the effect of an insulator barrier (amorphous carbon) on individual CNTs.[19] They found that the barrier layer increases the work function and the E_{th}. Apparently, the reduced E_{th} detected from our PMMA−CNT matrix is a different case. Thus we propose the following model to explain our results. Consider two MWCNTs a distance r apart from each other. The electric field imposed by an electron located in a nanotube on another electron located at a neighboring nanotube is given by

$$E = \left(\frac{q}{4\pi\varepsilon_0 r^2}\right) \quad (1)$$

where ε_0 is the permittivity of vacuum and q is the charge of electrons. When the spacing between these MWCNTs is filled by PMMA with a dielectric constant k = 3.4, the electric field $\boldsymbol{E}$ will become $\boldsymbol{E}'$

$$\boldsymbol{E}' = \left(\frac{q}{4\pi\varepsilon r^2}\right) = \left(\frac{q}{4\pi\varepsilon_0 k r^2}\right) \quad (2)$$

where $\varepsilon = \varepsilon_0 k$. Hence the electric field between two electrons in two neighboring nanotubes is reduced by the factor of k = 3.4 for the case of the PMMA−CNT matrix.

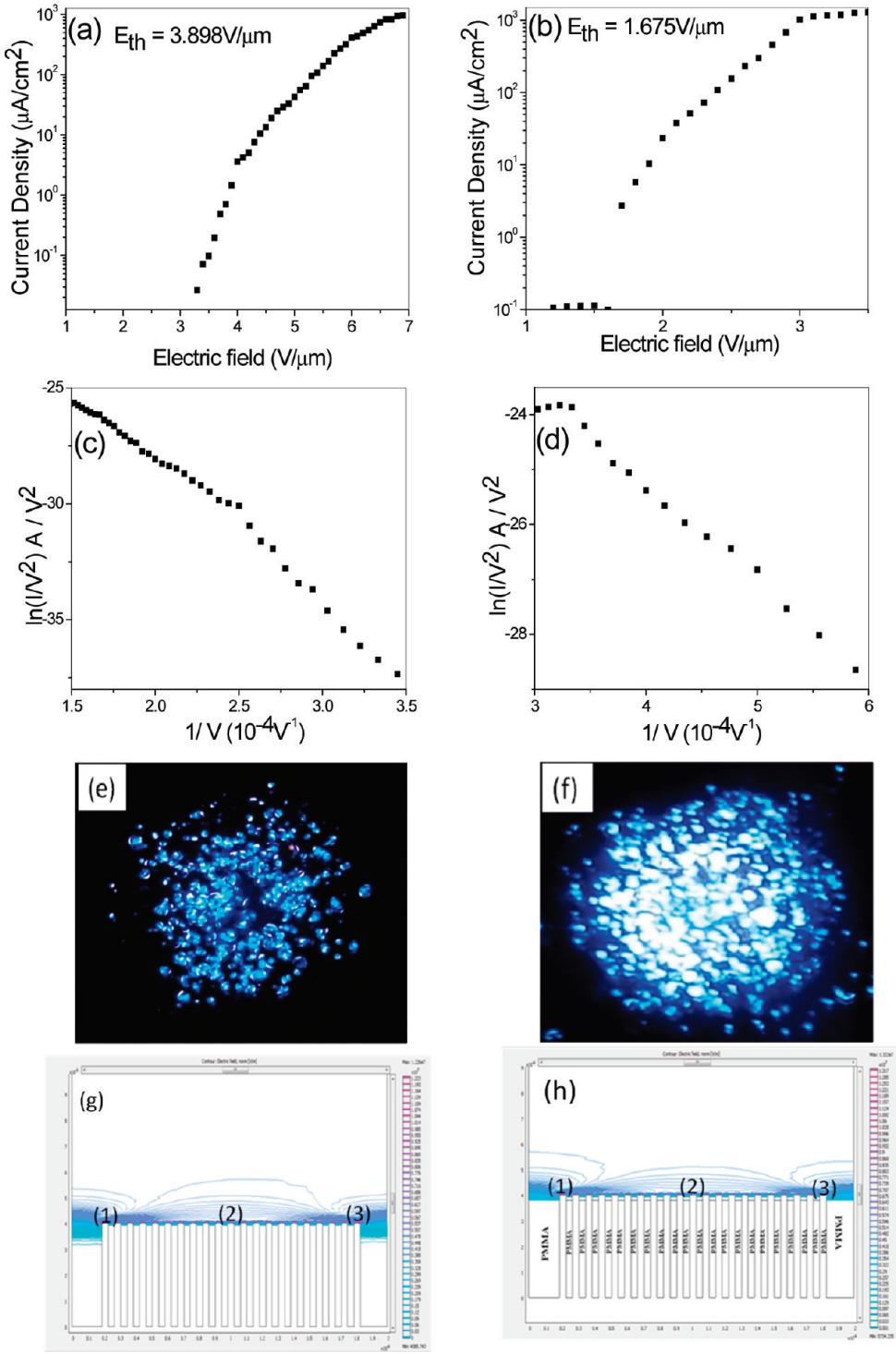

Figure 3. Emission current density (*J*) as a function of the applied electric field (*E*) for (a) the as-grown sample and (b) the PMMA−CNT matrix. The corresponding *F*−*N* plots for (c) as-grown sample and (d) the PMMA−CNT matrix. Images of the emission sites for (e) as-grown sample and (f) the PMMA−CNT matrix. The simulated potential maps for (g) the as-grown sample and (h) the PMMA−CNT matrix with exposed CNT tips.

Figure 4a,b indicates the schematic drawing of electron flows during electron field emission from the as-grown sample and the PMMA−CNT matrix, respectively. In this model, we consider that electron flows are driven by the electric forces ($\boldsymbol{F}_E$) generated by the applied electric field between the anode and the cathode. In addition, we also consider that electric field imposed by electrons in the neighboring MWCNTs will produce coulombic repulsion forces, $\boldsymbol{F}_e$ ($=q\mathbf{E}$, $\boldsymbol{E}$ = electric field in eq 1), in directions perpendicular to the driving force $\boldsymbol{F}_E$. This means that electron flows in individual MWCNTs will not simply go from the cathode to

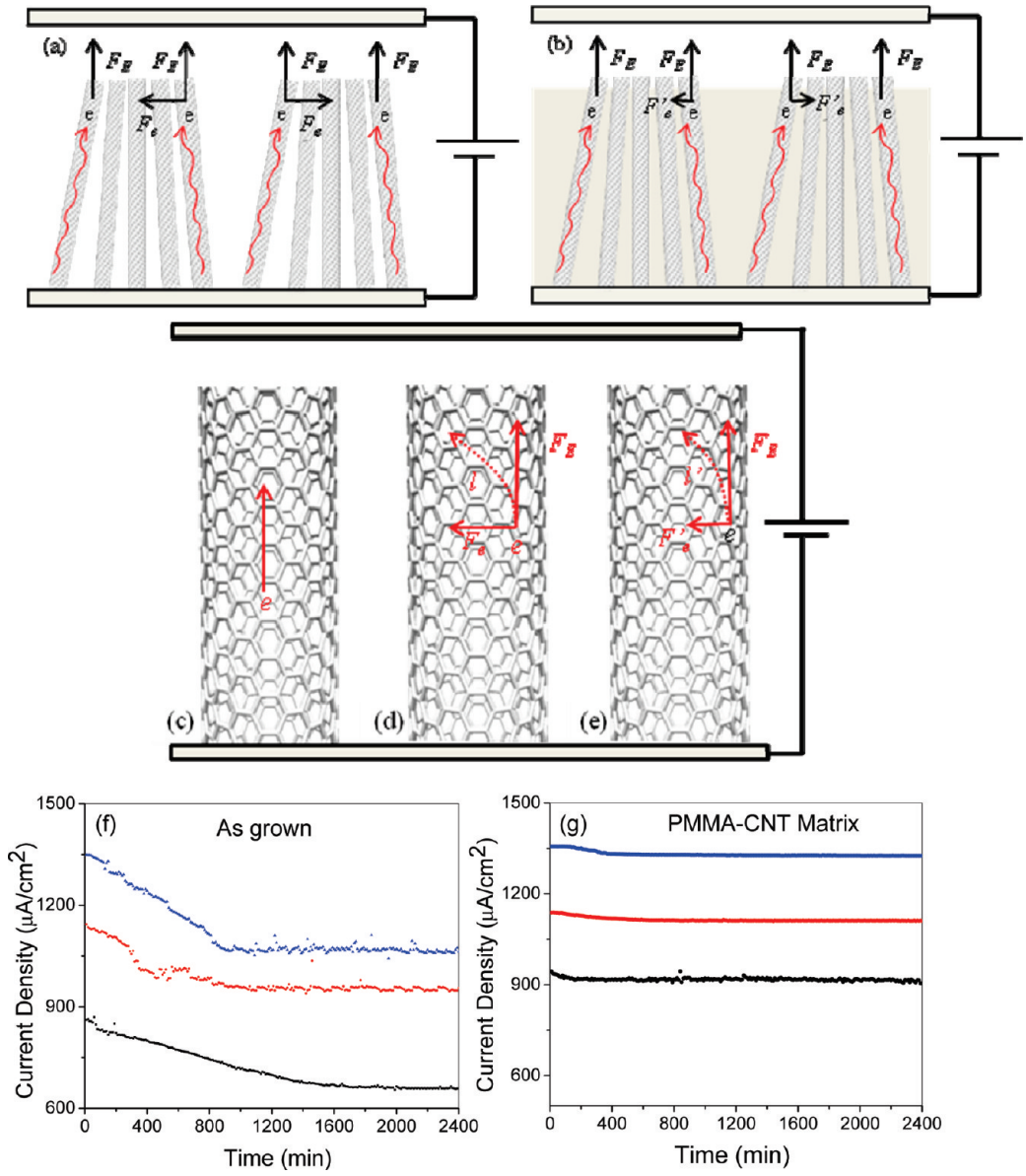

Figure 4. Schematic of electron flows in (a) the as-grown sample and (b) the PMMA−CNT matrix. Effective electron paths along (c) an isolated CNT, (d) an as-grown CNT with neighboring nanotubes, and (e) nanotubes in the PMMA−CNT matrix. Emission current as a function of time for (f) the as-grown sample and (g) the PMMA−CNT matrix at various initial current densities.

the anode (upward), but will be drifted left and right along the graphene sheets of the nanotubes due to the surrounding coulombic forces. For the case of the PMMA−CNT matrix, the drifting will be smaller due to the smaller $\boldsymbol{F}_e'$ ($=e\boldsymbol{E}'$, $\boldsymbol{E}'$ = electric field in eq 2).

The effective path length traveled by electrons before they reached the tips of nanotubes is explained here. For an isolated nanotube, electrons are driven only by the upward electric forces ($\boldsymbol{F}_E$) between the anode and the cathode, as shown in Figure 4c. In this case, the total distance traveled by the electrons before field emission is equal to the length of the nanotube. For nanotube films in our case, neighboring nanotubes are separated by tens of nanometers. In these cases, electric field $\boldsymbol{E}$ imposed by electrons in the neighboring MWCNTs will produce a coulombic force, $\boldsymbol{F}_e$, in directions perpendicular to the driving force, as shown in Figure 4d,e. For the as-grown sample, electrons flowing in a nanotube will drift following the dashed trajectory (l) in Figure 4d if there are electrons flowing in the neighboring nanotubes located on the right side. In this case, the actual distance traveled by the electrons before they reached the tip of the nanotube will be longer than the length of the nanotube. For the PMMA−CNT matrix, electric field $\boldsymbol{E}'$ ($|\boldsymbol{E}'| < |\boldsymbol{E}|$) will be imposed by electrons in the neighboring nanotubes and produce a coulombic force, $\boldsymbol{F}_e'$, as shown in Figure 4e. Since $|\boldsymbol{F}_e'| < |\boldsymbol{F}_e|$, electrons in this nanotube will travel in a trajectory path shorter (l') than that in the case of the as-grown sample illustrated in Figure 4d.

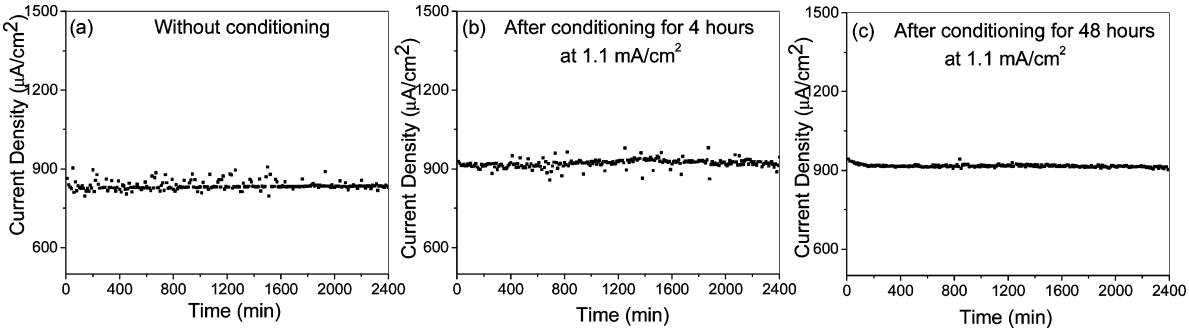

Figure 5. Emission current as a function of time for a PMMA−CNT matrix (a) before conditioning and after conditioning for (b) 4 h and (c) 48 h.

In reality, all MWCNTs are not defect-free. This means electron flows along MWCNTs will be scattered by defects and generate Joule heating. Thus the longer the electron drifting distance in nanotubes, the more Joule heating will be generated. Due to the smaller drifting and shorter effective travel distances, electrons in the PMMA−CNT matrix will generate less Joule heating. As previously reported, the emission stability depends on the electron scattering process along the nanotubes.[15] For the present study, since electron scattering is reduced for the PMMA−CNT matrices, better field emission stability is expected.

In order to verify this hypothesis, we have evaluated the emission stability of our samples. Figure 4f shows the emission stability curves measured from the as-grown sample at different initial current densities (~860, ~1140, ~1350 μA/cm^2). As shown, the emission current densities are degraded with time. Figure 4g shows the typical emission stability curves for the PMMA−CNT matrix. As shown, PMMA−CNT matrices are stable electron emitters as negligible degradation is detected within the 40 h continuous test. Similar trend has been detected from six sets of samples (see the data for another sample in Supporting Information). We think that the improvement in the emission stability of the PMMA−CNT matrix is due to *both* the reduction in screening effect and electron scattering (Joule heating). As the screening effect from surrounding CNTs is reduced, CNTs in the PMMA−CNT matrix can offer more emission sites and thus contribute to higher emission current and lower emission threshold field. The reduced Joule heating means reduced defect scattering along MWCNTs and thus enhances the current stability. It is noted that the stability data at ~900 μA/cm^2 in Figure 4g were obtained after conditioning as described hereafter.

As shown in Figure 5a, the emitted current is noisy when the matrix is tested at a current density below ~900 μA/cm^2. However, the overall current is stabilized at the initial value after the 40 h test. The noise is due to the presence of adsorbates,[21] which could be thermally desorbed when operating during electron emission. Our stability tests are started from low current density (following the sequence of ~860, ~1140, ~1350 μA/cm^2). Desorption rate of adsorbates is lower for the test at 860 μA/cm^2 due to lower Joule heating. It is possible that the desorption rate is comparable to the readsorption rate of adsorbates and leads to the noisy signals. Desorption rate is higher when the matrix is operated at higher emission currents (1140 and ~1350 μA/cm^2) and thus leads to lower noise, as shown in Figure 4g. This discussion is supported as follows. We have first conditioned the PMMA−CNT matrix by emitting current at ~1140 μA/cm^2 for 5 h and then redo the stability test at ~860 μA/cm^2. Figure 5b shows that the noise level is reduced. Then, we condition the sample again at ~1140 μA/cm^2 for 48 h. The stability test at ~860 μA/cm^2 is low in noise thereafter (Figure 5c). As discussed so far, all of the data in Figures 4 and 5 are collected from the same PMMA−CNT matrix. The cumulative stability test hour for the sample is more than 500 h so far and shows no sign of performance degradation. To further support our discussion, we have fabricated another PMMA−CNT matrix and conditioned the sample at ~1140 μA/cm^2 for 48 h. Then, stability tests at three different current levels (low to high) were completed. Results show that our PMMA−CNT matrices are stable electron emitters with reproducible stability (Supporting Information).

CONCLUSION

We found that PMMA−CNT matrices are excellent electron field emitters. The emission threshold field for 1 μA/cm^2 was reduced to 1.675 V/μm in comparison with 3.898 V/μm of the as-grown samples. The emission densities from the PMMA−CNT matrices are high, merely filling up the entire growth surface of the sample. We discussed the possible reasons behind this field emission improvement and attributed these enhancements to (1) the reduction in the screening effect from the neighboring CNTs due to dielectric properties of PMMA, as suggested by our theoretical simulation, and (2) reduced defect scattering and Joule heating due to the shorter effective transport distance of the electrons in MWCNTs. We have demonstrated stable emis-

sion at a level of 1350 μA/cm^2 continuously for 40 h. It is evidenced here that filling the spaces between CNTs with dielectric materials will lead to lower E_{th}, higher emission density, and better emission stability. This approach can be a promising method for fabricating practical electron field emitters.

METHODS

Synthesis of VA-MWCNTs. A dual radio frequency plasma enhanced chemical vapor deposition (PECVD) technique was used to prepare our VA-MWCNT samples. Our VA-MWCNTs were grown within a circular area of 0.385 cm^2 (7 mm in diameter). Up to three identical samples can be prepared in each growth process. For the present work, two identical samples were grown for each set of experiments. One sample serves as the as-grown sample and the other for the fabrication of a PMMA−CNT matrix. For CNT growth, Ni films with a thickness of 10 nm were deposited on p-type low resistance Si substrates by an RF magnetron sputtering technique. The catalyst-deposited substrates were loaded on a ceramic heater and inserted into the PECVD system. The chamber was evacuated to a base pressure of 1×10^{-3} mbar, and the CNTs were then grown at 450 °C for 1 h by using methane gas. The details of the growth procedures have been reported elsewhere.[20]

Preparation of PMMA−CNT Matrices and Field Emission Characterization. The fabrication scheme of the PMMA−CNT matrices using PMMA solution is summarized in Figure 1. The PMMA solution was prepared by diluting PMMA with the developer solution (Microchem) in a volume ratio of 1:1. As-grown VA-MWCNT samples (Figure 1a) were dipped into the solution for 15 min and followed by an annealing process at ~100 °C for 2−3 min. The cured samples (Figure 1b) were then mechanically polished by using fiber-free lapping cloth and a colloidal silica (0.02 μm in diameter) solution to expose the tips of the CNTs. The PMMA−CNT matrices with opened-tip CNTs will finally be formed (Figure 1c) and ready for the field emission measurements. Figure 1d shows the schematic of our field emission setup with indium tin oxide (ITO) coated on alumina silicate glasses as the anode. For the characterization of electron field emission, all samples were attached on the brass cathode in a planar diode configuration by applying a thin layer of silver paste. The spacing between the ITO anode and the tips of the CNTs was maintained at 1000 ± 10 μm. Electron emission was tested at a base vacuum pressure of ~1.5×10^{-8} Torr. The appearance of the as-grown sample and the PMMA−CNT matrix is shown in Figure 1e,f, respectively.

Acknowledgment. This work was supported by the Defense Advanced Research Projects Agency (Contract Number DAAD17-03-C-0115 through the U.S. Army Research Laboratory), and the U.S. Department of Army (Grant Number W911NF-04-1-0029). Contribution from B. Ulmen is appreciated.

Supporting Information Available: Field emission properties of another PMMA−CNT matrix are shown. This material is available free of charge *via* the Internet at http://pubs.acs.org.

REFERENCES AND NOTES

1. Rinzler, A. G.; Hafner, J. H.; Nikolaev, P.; Nordlander, P; Colbert, D. T.; Smalley, R. E.; Lou, L.; Kim, S. G.; Tománek, D. Unraveling Nanotubes: Field Emission from an Atomic Wire. *Science* **1995**, *269*, 1550.
2. de Heer, W. A.; Châtelain, A.; Ugarte, D. A Carbon Nanotube Field-Emission Electron Source. *Science* **1995**, *270*, 1179.
3. Collins, P. G.; Zettl, A. A Simple and Robust Electron Beam Source from Carbon Nanotubes. *Appl. Phys. Lett.* **1996**, *69*, 1969.
4. Choi, W. B.; Chung, D. S.; Kim, H. Y.; Jin, Y. W.; Han, I. T.; Lee, Y. H.; Jung, J. E.; Lee, N. S.; Park, G. S.; Kim, J. M. Fully Sealed, High-Brightness Carbon-Nanotube Field-Emission Display. *Appl. Phys. Lett.* **1999**, *75*, 3129.
5. Nilsson, O.; Groening, C.; Emmenegger, O.; Schaller, K. E.; Schlapbach, L.; Kind, H.; Bonard, J. M.; Kern, K. Scanning Field Emission from Patterned Carbon Nanotube Films. *Appl. Phys. Lett.* **2000**, *76*, 2071.
6. Kim, D. W.; Jin, S. Morphology Control of Patterned Carbon Nanofiber Arrays for Field Emission Applications. *J. Appl. Phys.* **2006**, *45*, 346.
7. Patole, S. P.; Patole, A. S.; Rhen, D. S.; Shahid, M.; Min, H.; Kang, D. J.; Kim, T. H.; Yoo, J. B. Patterned Carbon Nanotube Growth Using an Electron Beam Sensitive Direct Writable Catalyst. *Nanotechnology* **2009**, *20*, 315302.
8. Kanga, W. P.; Davidsona, J. L.; Wisitsora-ata, A.; Wonga, Y. M.; Takalkara, R.; Subramaniaa, K.; Kernsb, D. V.; Hofmeister, W. H. Diamond and Carbon-Derived Vacuum Micro- and Nano-electronic Devices. *Diamond Relat. Mater.* **2005**, *14*, 685.
9. Schvartzman, M.; Mathur, A.; Kang, Y.; Jahnes, C.; Hone, J.; Wind, S. J. Fluorinated Diamondlike Carbon Templates for High Resolution Nanimprint Lithography. *J. Vac. Sci. Technol. B* **2008**, *26*, 6.
10. Yi, W.; Jeong, T.; Yu, S. G.; Heo, J.; Lee, C.; Lee, J.; Kim, W.; Yoo, J. B.; Kim, J. Field Emission Characteristics from Wide-Bandgap Material-Coated Carbon Nanotubes. *Adv. Mater.* **2002**, *14*, 1464.
11. Watts, P. C. P.; Lyth, S. M.; Mendoza, E.; Silva, S. R. P. Polymer Supported Carbon Nanotube Arrays for Field Emission and Sensor Devices. *Appl. Phys. Lett.* **2006**, *89*, 103113.
12. Jo, S. H.; Tu, Y.; Huang, Z. P.; Carnahan, D. L.; Wang, D. Z.; Ren, Z. F. Effect of Length and Spacing of Vertically Aligned Carbon Nanotubes on Field Emission Properties. *Appl. Phys. Lett.* **2003**, *82*, 3520.
13. Jin, F.; Liu, Y.; Day, C. M.; Little, S. A. Enhanced Electron Emission from Functionalized Carbon Nanotubes with a Barium Strontium Oxide Coating Produced by Magnetron Sputtering. *Carbon* **2007**, *45*, 587.
14. Bonard, J. M.; Klinke, C. Degradation and Failure of Carbon Nanotube Field Emitters. *Phys. Rev. B* **2003**, *67*, 115406.
15. Kayastha, V. K.; Ulmen, B.; Yap, Y. K. Effect of Graphitic Order on Field Emission Stability of Carbon Nanotubes. *Nanotechnology* **2007**, *18*, 035206.
16. Pandey, A.; Prasad, A.; Moscatello, J.; Ulmen, B.; Yap, Y. K. Enhanced Field Emission Stability and Density Produced by Conical Bundles of Catalyst-Free Carbon Nanotubes. *Carbon* **2010**, *48*, 287.
17. Thomas, K. J.; Sheeba, M.; Nampoori, V. P. N.; Vallabhan, C. P. G.; Radhakrishnan, P. Raman Spectra of Polymethyl Methacrylate Optical Fibres Excited by a 532 nm Diode Pumped Solid State Laser. *J. Opt. A: Pure Appl. Opt.* **2008**, *10*, 055303.
18. Issac, A.; Borczyskowski, C. V.; Cichos, F. Correlation between Photoluminescence Intermittency of CdSe Quantum Dots and Self-Trapped States in Dielectric Media. *Phys Rev. B* **2005**, *71*, 161302.
19. Tanaka, H.; Akita, S.; Pan, L.; Nakayama, Y. Barrier Effect on Field Emission from Stand-Alone Carbon Nanotube. *J. Appl. Phys.* **2004**, *43*, 864.
20. Menda, J.; Ulmen, B.; Vanga, L. K.; Kayastha, V. K.; Yap, Y. K.; Pan, Z.; Ivanov, I. N.; Puretzky, A. A.; Geohegan, D. B. Structural Control of Vertically Aligned Multiwalled Carbon Nanotubes by Radio-Frequency Plasmas. *Appl. Phys. Lett.* **2005**, *87*, 173106.
21. Purcell, S. T.; Vincent, P.; Journet, C; Binh, V. T. Hot Nanotubes: Stable Heating of Individual Multiwall Carbon Nanotubes. *Phy. Rev. Lett.* **2002**, *88*, 105502.